Nanoscale spin structures dominated by magnetoelastic interactions around dislocation cores as seen via spin-polarized STM

Luis Berbil-Bautista,[1] Stefan Krause,[2] Matthias Bode,[3] Antonio Badía-Majós,[4] César de la Fuente,[4] Roland Wiesendanger,[2] and José Ignacio Arnaudas[5]

[1]*Materials Sciences Division, Lawrence Berkeley National Laboratory, Berkeley, California 94720-7300, USA*

[2]*Institute of Applied Physics, University of Hamburg, Jungiusstr. 11, D-20355 Hamburg, Germany*

[3]*Center for Nanoscale Materials, Argonne National Laboratory, Argonne, Illinois 60439, USA*

[4]*Departamento de Física de la Materia Condensada and Instituto de Ciencia de Materiales de Aragón,*

Universidad de Zaragoza and CSIC, 50071 Zaragoza, Spain

[5]*Departamento de Física de la Materia Condensada and Instituto de Nanociencia de Aragón, Universidad de Zaragoza,*

50071 Zaragoza, Spain

We report on studies of spin structures that appear around screw and edge dislocations in Dy (0001) films grown on W (110) substrates. By means of spin-polarized scanning-tunneling microscopy, we have observed the formation of vortexlike and lobe-shaped magnetic structures. We have studied the effect of fundamental dislocations in micromagnetic simulations by including the magnetoelastic interactions in addition to the usually considered energy terms which arise from the magnetocrystalline anisotropy and the exchange energies. Starting from actual physical parameter values for Dy, our calculations are in qualitative and quantitative agreement with the size and the shape of the spin structures experimentally observed.

PACS number(s): 75.70.−i, 68.37.Ef, 75.80.+q

The influence of structural defects on nanoscale magnetic properties is not only of fundamental but also of applied interest as a detailed understanding may be crucial for developing ultrahigh-density magnetic recording media. For example, previous experiments on Pt/Co/Pt trilayers have shown that the strain associated with linear defects efficiently controls domain wall pinning via the magnetoelastic (ME) interaction, with only a few of such defects needed to stabilize the large area domain structure of ultrathin films.[1] Rare-earth (RE) metals are of great interest for studies of the ME interaction since it is particularly strong in this material class and since multilayers consisting of RE metals and transition metals are used as magneto-optical recording systems.[2] In this context, it is worth noting that previous studies have shown that the "large scale" magnetic structure of Dy films on W (110) is dominated by the density of linear defects that evolve during film growth.[3,4]

Particularly, strong magnetostrictive effects can be expected several tens of nanometers around the core of a dislocation, i.e., at distances smaller than the corresponding decay length of the strain fields in metals. At this length scale, the magnetic structure should be governed by the competition between exchange coupling and ME interaction. Since a thorough investigation requires the direct correlation of structural and magnetic properties on a lateral scale well below 50 nm, spin-polarized scanning-tunneling microscopy (SP-STM) appears as the ideal tool.

The SP-STM experiments were performed in an ultrahigh-vacuum system at temperatures between 20 and 60 K. To obtain magnetic contrast the tips were coated with at least 100 atomic layers (ALs) of antiferromagnetic Cr, as described in Ref. 5, or dipped into the Dy film to obtain a Dy cluster on the tip apex, as described in Ref. 4. These two methods result in tips preferentially magnetized parallel to the sample's surface plane.[4,6,7] The magnetic signal was mea-sured by mapping the spin-resolved differential tunneling conductance dI/dU as a function of lateral position of the tip. This dI/dU signal was recorded by lock-in detection of the current modulation that results from adding a modulation voltage $U_{mod}=25$ mV$_{rms}$ to the sample bias and is proportional to the projection of the local magnetization of the sample, m_s, onto the tip magnetization, m_t, at any given position of the surface.[8,9]

Continuous and flat (0001) terminated Dy films were grown on W (110) following the process described in Ref. 4. We have shown that these Dy films exhibit a ferromagnetic surface layer with magnetic domains in six in-plane directions at temperatures below the Curie temperature of bulk Dy.[3,4] Figure 1(a) shows an STM topograph of such a 90 AL film of Dy. The surface presents monoatomic steps that separate atomically flat terraces. Two steps always merge at the position where a screw dislocation with a Burgers vector [0001] pierces the surface (white arrows in Fig. 1).[3] Within the atomically flat terraces highly asymmetric depressions are found that—by means of atomically resolved STM—were identified as the point where edge dislocations with a Burgers vector $[2\bar{1}\bar{1}0]$ emerge to the surface.[3] In Fig. 1 these positions are marked by circles. The comparison of the positions of the line defects observed in the STM topograph in Fig. 1(a) with the magnetic signal map in Fig. 1(b) reveals that both kinds of defects result in strong pinning of the domain walls.[3] In most cases, several domains meet at the position of the pinning center, as, e.g., in the lower right corner of Fig. 1(b), where three domains meet at the position of an edge dislocation. These patterns often resemble the spin structure previously observed around magnetic vortex cores[6] with a continuous in-plane magnetization in close proximity to the dislocation site. Occasionally, another feature consisting of a lobelike structure surrounded by a single ferromagnetic domain are found, as the one marked with a
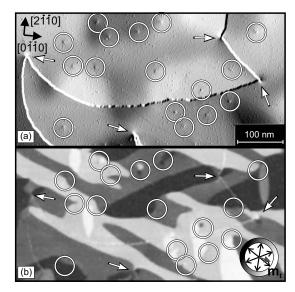
FIG. 1. (a) STM topograph and (b) magnetic signal map of a 90 AL Dy film. The schematic inset summarizes the different magnetic contrast levels which result from different projections of m_s onto m_t calculated as in Ref. 4, The arrows (circles) mark the position where screw (edge) dislocation appear on the surface.

gray arrow in Fig. 1(b). Both features are discussed in greater detail in Figs. 2 and 3, respectively.

Figure 2 shows a close view of the topography and the spin structure of typical screw (top panels) and edge dislocations (bottom panels). The structural line defects are marked by hatched circles in the topographs. Figure 2(b) clearly reveals that four different domains meet at the position of the screw dislocation. A vortexlike structure emerging form the dislocation position is observed in the inset. The plot in Fig. 2(c) shows a circular line section along the circle in Fig. 2(b) with the origin at the intersection of the circle and the radial line taken counterclockwise (CCW) as indicated by the arrow. The circular line section is taken at a diameter of 7.1 nm. The magnetization changes smoothly and no plateaus are present. The jumps in the magnetic sig-
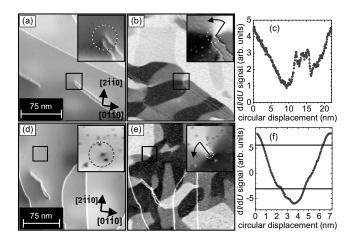

FIG. 2. [(a) and (d)] STM topographs and [(b) and (e)] magnetic signal maps of typical screw and edge dislocations, respectively. (c) and (f) are the circular line sections marked in the insets of (b) and (e).
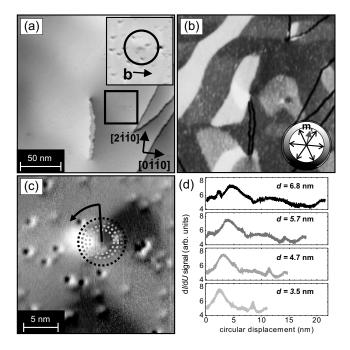

FIG. 3. (a) STM topograph and (b) magnetic signal map of a region where an edge dislocation is localized within a single domain. (c) Detail of the neighborhood of the dislocation. (d) Circular line sections marked in (c).

nal are due to a different spin-averaged electronic structure at the step edges.

In the case of the edge dislocation shown in the topograph in Fig. 2(d), the magnetic signal map of Fig. 2(e) reveals that five different domains are pinned at the dislocation. Again, this results in a smooth variation in the magnetization with no plateaus, as shown in the circular line section of the magnetic signal taken at a diameter of 2.4 nm from the core of the dislocation displayed in Fig. 2(e). In both cases the behavior clearly resembles the continuous spin rotation observed around a magnetic vortex core.[6] The horizontal lines in the plot represent the magnetic signal of the brightest and the darkest domains, i.e., the domains with largest parallel and antiparallel component of m_s relative to m_t, respectively. Obviously, the magnetic signal around the core of the dislocation exceeds these values. This is due to the fact that close to the dislocation m_s is no longer pinned along the six equivalent easy axes of Dy (0001) but rather continuously rotates within the surface layer. As a consequence there is a position where m_s is truly (anti)parallel with m_t resulting in a maximum magnetic signal.

As mentioned above, in some cases, edge dislocations are located within a single domain as in the case of Fig. 3. Panel 3(a) shows the topography of the area. The direction of the dislocation Burgers vector is indicated in the inset. This direction has been determined by the comparison of the asymmetric shape of the depression of the dislocation core with the previously analyzed atomically resolved STM topographs of similar defects (cf. Ref. 3). Figure 3(b) shows a magnetic signal map taken simultaneously with Fig. 3(a). The schematic inset summarizes the different magnetic contrast levels which result from different projections of m_s onto m_t. Based on the analysis presented in Ref. 4, we obtain an

angle of $98 \pm 5°$ between the magnetization direction of the large domain in the square and m_t. The closer view in Fig. 3(c) shows that a single insulated dark-bright lobe structure emerges from the dislocation core. It extends about 10 nm into the surrounding domain. The circular line sections of the magnetic signal taken at different distances from the dislocation core shown in Fig. 3(d) reveal a continuous behavior of the magnetic signal with extremes of the canting angles in the lobes of $45 \pm 15°$ and $170 \pm 15°$ in the brightest and the darkest regions.

In order to interpret the observed magnetic structures and to analyze the driving forces generated by the linear defect, we have calculated the spin directions of an ensemble of atoms surrounding an edge dislocation. In physical terms, the interaction between the stress field occurring around a dislocation line and the spontaneous magnetostrictive strains existing in a ferromagnet gives rise to a ME energy which, together with exchange, dipolar, anisotropy, and elastic energies, determine the magnetic configuration in the neighborhood of the linear defect. In uniformly strained materials, the distortion of the lattice tends to align the magnetic moments along certain directions. However, as we shall see below, the nonuniform stress field of the dislocation results in a canting of the magnetic moments near the dislocation core. Previous theoretical studies (see, e.g., Ref. 10, further references therein) have addressed the role of dislocations and other lattice defects on collective properties such as the dependence of the coercive field on the domain wall thickness. In the present work we will focus on the determination of the local spin arrangement in close proximity to an edge dislocation, and we will compare our simulations with the observed magnetic structures.

In our calculation we consider a ferromagnetic domain in a Dy film, having its magnetization parallel to one of the easy magnetization axes (**a** directions) in the basal plane (BP) of the Dy hexagonal close packed (hcp) crystal structure. We assume a single edge dislocation with Burgers vector $\vec{b}=[2\bar{1}\bar{1}0]a$ and a dislocation line running perpendicular to the BP through the whole film thickness. The numerical study of the spin configuration was performed by using an hcp arrangement of magnetic ions and considering translational symmetry along the direction perpendicular to the film plane, i.e., to the BP of the hcp structure. An hexagonal two-dimensional (2D) lattice consisting of a set of ion sites was used. In the center of the mesh we define the origin of a Cartesian coordinate system (OXY), where the core of a pure edge dislocation running along the z axis is located. This extra plane located at $y > 0$ produces a stress field which essentially compresses the upper half of the mesh and tenses the lower one. The stress field produced by this linear defect depends on the crystal structure. For an hexagonal crystal the non-null components of the stress tensor, $\overset{\leftrightarrow}{\sigma}(\mathbf{r})$, are (see, e.g., Ref. 11), $\sigma_{xx}=-y(ax^2+by^2)/u(x,y)$, $\sigma_{yy}=y(gx^2-hy^2)/u(x,y)$, $\sigma_{xy}=\sigma_{yx}=x(ex^2-fy^2)/u(x,y)$, and $\sigma_{zz}=y(px^2+qy^2)/u(x,y)$, where $u(x,y)=x^4+sx^2y^2+ty^4$ and the coefficients of the x and y coordinates are combinations of the hexagonal elastic constants of the material and include the Burger's vector modulus, $|\vec{b}|=b_x=3.2$ Å, in our case. This strongly anisotropic stress field which decays with dis-

tance ($\sigma_{ij} \propto 1/r$) couples with the magnetization via the ME interaction and can be described by a local anisotropy field which is to be added to the magnetocrystalline anisotropy. Thus, the free energy of a layer of Dy ions can be written as the sum of: (i) basal-plane anisotropy energy, F_{CEF} which originates from the crystal electric field (CEF), (ii) the ME energy, F_{ME}, associated with the non-null strains, (iii) the dipolar energy, F_D, and (iv) the exchange energy, F_{EX}. As a first approximation, $F_{CEF} \simeq \Sigma_i K_6^6 \cos(6\varphi_i)$, where K_6^6 is the hexagonal BP pure CEF anisotropy constant and φ_i is the angle formed by the ith spin direction and the hcp easy axis, **a**. The ME energy per ion, located at $\mathbf{r}_i$, may be written in the form $-\overset{\leftrightarrow}{\epsilon}(\mathbf{r}_i):\overset{\leftrightarrow}{\sigma}(\mathbf{r}_i) \equiv -\Sigma_{kl}\epsilon_{kl}(\mathbf{r}_i)\sigma_{kl}(\mathbf{r}_i)$, where $\overset{\leftrightarrow}{\epsilon}(\mathbf{r}_i)$ is the local magnetostrictive strain tensor which depends on the strength of the ME interaction and on the spin direction at $\mathbf{r}_i$ (Ref. 12) and $\overset{\leftrightarrow}{\sigma}(\mathbf{r}_i)$ is the internal stress tensor caused by the dislocation. In our case $F_{ME}=-\Sigma_i[\lambda_{100}(\sigma_{xx}^i \cos^2 \varphi_i+\sigma_{xy}^i \sin 2\varphi_i +\sigma_{yy}^i \sin^2 \varphi_i)+\lambda_{101}\sigma_{zz}^i]$, where λ_{100} and λ_{101} are magnetostriction constants. The classical dipolar interaction gives rise to the energy $F_D=(\mu_0/4\pi)g^2\mu_B^2\Sigma_{i>j}\{[\mathbf{J}_i \cdot \mathbf{J}_j]r_{ij}^{-3} -3[(\mathbf{J}_i \cdot \mathbf{r}_{ij})(\mathbf{J}_j \cdot \mathbf{r}_{ij})]r_{ij}^{-5}\}$, where $\mathbf{r}_{ij}$ is the vector between spin sites i and j, μ_0 is the permeability of the vacuum, g is the Landé factor (4/3 for Dy), J is the total angular momentum (15/2 for Dy), and μ_B is the Bohr magneton. Finally, $F_{EX}=-(\mathfrak{I}/2)\Sigma_{i,j}^*\mathbf{J}_i \cdot \mathbf{J}_j$, $\mathfrak{I}$ being the ferromagnetic exchange constant and the symbol "*" indicating that each ion is exchange coupled only to its six nearest neighbors.

Minimization of the total energy $F_{CEF}+F_{ME}+F_D+F_{EX}$ allows us to obtain the equilibrium configurations of magnetic momenta around the edge dislocation. As constraints we used periodic boundary conditions with a fixed moment direction at the sample boundaries and constant modulus for all atomic sites. This means that we are analyzing the effect of an edge dislocation located in the center of a single magnetic domain with equal spins which would be otherwise ferromagnetically aligned along one of the easy directions, **a**. Then, by using the normalized magnetic moments $\mathbf{m}_i=(\cos \varphi_i\hat{x},\sin \varphi_i\hat{y})$, the numerical simulation starts from the simplified expression for the free energy $F=K_6^6\Sigma_i(32m_{i_x}^6-48m_{i_x}^4+18m_{i_x}^2)-\Sigma_i\mathbf{m}_i^T C(\mathbf{r}_i)\mathbf{m}_i +\Sigma_{\alpha,\beta=x,y}\Sigma_{i>j}m_{i_\alpha}D_{\alpha\beta}^{ij}m_{j_\beta}-(\mathfrak{I}/2)J^2\Sigma_{i,j}^*\mathbf{m}_i^T\mathbf{m}_j$, where $\mathcal{J}=(J^2/2)\mathfrak{I}$ and the position dependent matrix C has the non-null elements: $C_{xx}=\sigma_{xx}\lambda_{100}$, $C_{yy}=\sigma_{yy}\lambda_{100}$, $C_{xy}=C_{yx}=\sigma_{xy}\lambda_{100}$, and $C_{zz}=\sigma_{zz}\lambda_{101}$, the latter giving a null contribution to F because the magnetization lies within the BP, and $D_{\alpha\beta}^{ij}=(\mu_0/4\pi)(g\mu_BJ)^2(\delta_{\alpha\beta}r_{ij}^{-3}-3r_{ij_\alpha}r_{ij_\beta}r_{ij}^{-5})$ are the dipole-dipole interaction coefficients. The variational problem has been solved numerically by means of the FORTRAN package LANCELOT that implements a globally convergent augmented Lagrangian algorithm[13] that allows to avoid spurious local minima. Since the studied Dy film, at $T=58$ K, clearly displays ferromagnetic order within the BP, the calculations have been performed by using the values of $\mathfrak{I}$, K_6^6, and λ_{100} of bulk Dy, i.e., $\mathfrak{I}=1.8 \times 10^7$ erg/cm^3,[14] $K_6^6=-3.0 \times 10^6$ erg/cm^3,[15] and $\lambda_{100}=8.1 \times 10^{-3}$.[16] The elastic constants appearing in the coefficients of the components of the stress tensor, $\overset{\leftrightarrow}{\sigma}(\mathbf{r}_i)$, are taken from Ref. 17.

The minimization of the free energy F leads to magnetic domains which extend indefinitely from the dislocation core
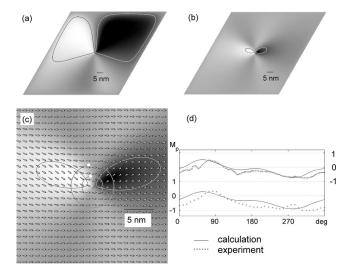
FIG. 4. (a) Calculated dI/dU map, using a 250×250 lattice, corresponding to the experimental conditions in Fig. 3. Two level contours are marked upon the lobes for visual purpose. (b) The same as for (a), with stabilizing field (see text for details). (c) Vector plot of the theoretical magnetic moments in the vicinity of the edge dislocation [75×75 sites, central part of (b)]; for clarity, a simplified mesh is represented. Panels (d) correspond to the circular CCW line sections, in the horizontal axis the angle in degrees starting from the white dots and in the vertical axis the magnetic signal in arbitrary units, shown in (c), at $d=7$ nm and $d=3.5$ nm.

[see Fig. 4(a), where the projection of the Dy spins onto m_t corresponding to the experimental conditions in Fig. 3 is plotted]. This result, which does not depend on the size of the 2D lattice up to 250×250 ion sites, does not explain the relatively small size of the structure shown in Fig. 3. Only after adding a Zeeman energy equivalent to the effect of an in-plane magnetic field of about 1 kOe to the free energy F,

we were able to reproduce the experimental finding of Fig. 3.

A possible origin of this in plane magnetic field may be the magnetic sandwich structure of Dy films on W (110). Indeed, it has been observed by means of resonant soft x-ray scattering in a 180 AL Dy film on W (110) that the low temperature ($T<125$ K) magnetic profile of the film is rather complex.[18]

Figure 4(b) shows the results of the new calculation and Fig. 4(c) shows the direction of the spins in a 75×75 ion sites region. The calculation recovers the extension of the observed magnetic structure and its general shape. Furthermore, Fig. 4(d) shows direct comparison of the magnetic signal from the experimental data and the calculated one, for two circular line sections at $d=7$ nm and $d=3.5$ nm. The agreement is quite good, particularly if we consider that in the parts where deviations occur we observe (see Fig. 3) the presence of adsorbates in the sample that clearly distort the magnetic image. The extrema of the magnetization canting angles in the calculation are 58° and 138° and are in reasonable agreement with the previously mentioned experimental values (notice that these extrema are located at around 61° and 280° in the circular line sections of Fig. 4).

In summary, the nanoscale magnetic structure around single line defects in Dy/W (110) films has been studied by means of SP-STM and micromagnetic calculations. The presence of complex spin structures can be quantitatively explained by the strong changes in magnetic easy axis driven by the coupling of the magnetoelastic energy and the deformation field around the dislocation core.

[1] L. Krusin-Elbaum, T. Shibauchi, B. Argyle, L. Gignac, and D. Weller, Nature (London) **410**, 444 (2001).

[2] S. Tsunashima, J. Phys. D **34**, R87 (2001).

[3] S. Krause, L. Berbil-Bautista, T. Hänke, F. Vonau, M. Bode, and R. Wiesendanger, Europhys. Lett. **76**, 637 (2006).

[4] L. Berbil-Bautista, S. Krause, M. Bode, and R. Wiesendanger, Phys. Rev. B **76**, 064411 (2007).

[5] M. Bode, Rep. Prog. Phys. **66**, 523 (2003).

[6] A. Wachowiak, J. Wiebe, M. Bode, O. Pietzsch, M. Morgenstern, and R. Wiesendanger, Science **298**, 577 (2002).

[7] A. Kubetzka, M. Bode, O. Pietzsch, and R. Wiesendanger, Phys. Rev. Lett. **88**, 057201 (2002).

[8] J. C. Slonczewski, Phys. Rev. B **39**, 6995 (1989).

[9] D. Wortmann, S. Heinze, P. Kurz, G. Bihlmayer, and S. Blügel, Phys. Rev. Lett. **86**, 4132 (2001).

[10] A. Seeger, H. Kronmüller, and H. Träuble, J. Appl. Phys. **35**, 740 (1964).

[11] J. P. Hirth and J. Lothe, *Theory of Dislocations* (Krieger, Malabar, FL, 1992).

[12] E. Callen and H. B. Callen, Phys. Rev. **139**, A455 (1965).

[13] A. R. Conn, N. I. M. Gould, and P. L. Toint, *LANCELOT: A Fortran Package for Large-Scale Nonlinear Optimization*, Springer Series in Computational Mathematics (Springer, New York, 1998).

[14] J. Jensen and A. R. Mackintosh, *Rare-Earth Magnetism: Structure and Excitations* (Clarendon press, Oxford, 1991).

[15] S. H. Liu, D. R. Behrendt, S. Legvold, and J. R. H. Good, Phys. Rev. **116**, 1464 (1959).

[16] J. J. Rhyne, in *Magnetic Properties of Rare-Earth Metals*, edited by R. J. Elliot (Plenum Press, New York, 1972), pp. 129–185.

[17] S. B. Palmer and E. W. Lee, Proc. R. Soc. London, Ser. A **327**, 519 (1972).

[18] H. Ott, C. Schßüler-Langeheine, E. S. G. Kaindl, and E. Weschke, Appl. Phys. Lett. **88**, 212507 (2006).